Contract No.:

This manuscript has been authored by Savannah River Nuclear Solutions (SRNS), LLC under Contract No. DE-AC09-08SR22470 with the U.S. Department of Energy (DOE) Office of Environmental Management (EM).

Disclaimer:

Anion-exchanged and quaternary ammonium functionalized MIL-101-Cr metal-organic framework (MOF) for ReO_4^-/TcO_4^- sequestration from groundwater

Dien Li[a,*], Natalia B. Shustova[b], Corey R. Martin[b], Kathryn Taylor-Pashow[a], John C. Seaman[c], Daniel I. Kaplan[a], Jake W. Amoroso[a], Roman Chernikov[d]

[a] Savannah River National Laboratory, Aiken, SC 29808, USA

[b] Department of Chemistry and Biochemistry, University of South Carolina, Columbia, SC 29208, USA

[c] Savannah River Ecology Laboratory, University of Georgia, Aiken, SC 29802, USA

[d] Canadian Light Source, Saskatoon, SK S7N 0X4, Canada

[*] Corresponding author.

Email: Dien.Li@srs.gov (D. Li).

ABSTRACT: There are few effective technologies for the sequestration of highly water-soluble pertechnetate (TcO_4^-) from contaminated water despite the urgency of environmental and public health concerns. In this work, anion exchanged and cetyltrimethylammonium bromide (CTAB) functionalized MIL-101-Cr-NO_3 were investigated for perrhenate (ReO_4^-), a surrogate of TcO_4^-, sequestration from artificial groundwater. Cl^-, I^-, and $CF_3SO_3^-$ exchanged MIL-101-Cr proved more effective at ReO_4^- removal than the parent MIL-101-Cr-F. Compared to the parent framework, CTAB functionalized MIL-101-Cr-NO_3 increased ReO_4^- removal capacity from 39 to

139 mg/g, improved the reaction kinetics from ~30 to < 10 minutes to reach full adsorption capacity and the selectivity for ReO_4^- over competing NO_3^-, CO_3^{2-}, SO_4^{2-}, and Cl^-. Spectroscopic data indicated that the chemical speciation of Re in the exchanged MIL-101-Cr remained ReO_4^-, indicating synergistic sequestration through both anion exchange and non-ion exchange binding with the positively charged ligand of CTAB. These studies foreshadow potential applications of MOFs for the remediation of $^{99}TcO_4^-$ from contaminated environments.

Keywords: Pertechnetate, Perrhenate, CTAB functionalization, MIL-101-Cr, Sequestration

1. Introduction

Pertechnetate (TcO_4^-) is the most common Tc contaminant species found at nuclear waste storage and management sites. It is highly water-soluble and mobile, and presents challenges for its sequestration (Icenhower et al., 2010; Meena and Arai, 2017). Previous methodologies for removal of TcO_4^- such as ion-exchange resins, layered double hydroxides, granular activated carbon, and organoclay materials have been employed with limited TcO_4^- loading capacities from aqueous media (Daniels et al., 2019; Gu et al., 2000; Li et al., 2019; Valenta et al., 2010). An alternative approach for TcO_4^- immobilization is the use of reducing agents (e.g., zero-valent iron, iron sulfides, stannous chloride, and reducing bacteria) (Darab et al., 2007; McBeth et al., 2011; Pierce et al., 2010; Plymale et al., 2011). Recently, studies indicated that TcO_4^- can be reduced to form Tc-sulfide phases (Asmussen et al., 2018; Fan et al., 2013; Pearce et al., 2018) or incorporated into a Fe(OOH) structure or corroded steel (Liu et al., 2012) through reductive co-precipitation (Um et al., 2011). There are also several studies to demonstrate that perrhenate (ReO_4^-), a non-radioactive chemical analog for TcO_4^-, can be incorporated into a sodalite structure (Dickson et

al., 2015; Pierce et al., 2017). However, removing TcO_4^- from environmental systems remains a largely unsolved challenge, and new technologies are required for Tc sequestration and nuclear waste treatment to minimize any potential risk to the environment and human health.

In comparison to other porous materials, metal-organic frameworks (MOFs) may prove to be an exceptional material for TcO_4^- sequestration due to their tunable pore sizes, impressively high surface areas, unprecedented modularity, and recyclability (Furukawa et al., 2010; Howarth et al., 2017; Yaghi et al., 1998). MOFs have been investigated over the last two decades primarily for gas adsorption (e.g., hydrogen storage, acetylene separation, and carbon dioxide capture), light harvesting and energy storage, efficient sensors, catalysis, and drug-delivery systems (Furukawa et al., 2013; Li et al., 2012). Recently, zeolitic imidazolate frameworks (ZIFs), zirconium-based frameworks, and several other MOFs have demonstrated chemically stability in aqueous media over a wide pH range 0−14 (Bosch et al., 2014; Howarth et al., 2016a; Wang et al., 2016), and have a high capacity for removing arsenate, selenate and selenite, sulfate, and other oxyanions from aqueous systems (Deng et al., 2019; Desai et al., 2016; Howarth et al., 2015a; Howarth et al., 2015b; Howarth et al., 2016b). These recent findings open a very attractive avenue for MOF applications for environmental remediation of various contaminants (Mon et al., 2018) and nuclear waste treatment (Banerjee et al., 2016b; Dolgopolova et al., 2018). More recently, several MOFs (Banerjee et al., 2016a; Banerjee et al., 2016c; Drout et al., 2018; Fei et al., 2011; Li et al., 2017b; Mei et al., 2019; Rapti et al., 2018; Sheng et al., 2019; Sheng et al., 2017; Xu et al., 2019; Zhu et al., 2017a) and cationic organic framework (Da et al., 2019; Ding et al., 2020; He et al., 2019; Li et al., 2018; Liu and Han, 2020; Samanta et al., 2018; Shen et al., 2017; Sun et al., 2019; Zhu et al., 2017b) have demonstrated the ability to trap ReO_4^- from aqueous media.

The overarching objective of the present study is to investigate the effects of anions (e.g., NO_3^-, F^-, Cl^-, I^-, and triflate group ($CF_3SO_3^-$)) and cetyltrimethylammonium bromide (CTAB) functionalized MIL-101-Cr (MIL, Matérial Institut Lavoisier) for ReO_4^-/TcO_4^- sequestration from groundwater under natural oxic conditions. The chemical formula of MIL-101-Cr is $Cr_3NO_3(H_2O)_2O(BDC)_3 \cdot nH_2O$ ($n \sim 25$; BDC = 1,4-benzenedicarboxylate; NO_3^- can be substituted by F^-, Cl^-, I^-, or $CF_3SO_3^-$). The chromium terephthalate metal–organic framework or MIL-101-Cr comprises of trimeric chromium(III) octahedral clusters interconnected by 1,4-benzenedicarboxylates, resulting in a highly porous 3-dimentional structure (Fig. 1). This makes it an ideal MOF material for contaminant treatment studies. More specifically, MIL-101-Cr materials were synthesized and characterized via a series of analytical techniques, including powder X-ray diffraction (PXRD), scanning electron microscopy (SEM) coupled with energy dispersive X-ray spectroscopy (EDS), Fourier-transform infrared spectroscopy (FTIR), and thermogravimetric analysis (TGA). The CTAB-functionalized MIL-101-Cr framework was extensively evaluated for its removal capacity of ReO_4^-, including the effects of reaction time, solution pH values, as well as the impact of coexisting anions on ReO_4^- adsorption, desorption, and resorption behavior using batch experiments. The MIL-101-Cr frameworks were further characterized after ReO_4^- adsorption by PXRD, FTIR, EDS, Re L_3-edge X-ray absorption near-edge structure (XANES), and extended X-ray absorption fine structure (EXAFS) spectroscopy to understand their hydrolytic stability, Re chemical speciation, and binding mechanisms within the MIL-101-Cr matrix. The batch experiments were conducted primarily using an artificial groundwater, if not specified, under oxidative conditions. Perrhenate (ReO_4^-) was chosen as a surrogate for TcO_4^- to evaluate its adsorption behavior because of their similar physiochemical

properties (e.g., oxidation states, ionic radius, and energy of hydration) (Darab and Smith, 1996; Icenhower et al., 2010).

2. Materials and Methods

2.1 MIL-101-Cr synthesis

Chromium(III) nitrate nonahydrate (98.5%, Beantown Chemical), aluminum(III) chloride hexahydrate (99%, Alfa Aesar), aluminum(III) iodide (95%, Strem Chemicals), aluminum(III) trifluoromethanesulfonate (99%, Oakwood Chemical), terephthalic acid (99%, TCI Chemicals), cetyltrimethylammonium bromide (99%, Oakwood Chemical) hydrofluoric acid (48%, Oakwood Chemical), nitric acid (70%, Sigma-Aldrich), *N*,*N*-dimethylformamide (ACS grade, BDH), chloroform (ACS grade, BDH), ethanol (200 proof, Decon Laboratories, Inc) were used as received. MIL-101-Cr-NO_3 and MIL-101-Cr-F was prepared by modified literature procedures (Skobelev et al., 2013; Zhao et al., 2015). A modified anion-stripping procedure was used to functionalize MIL-101-Cr-F with Cl, I, and triflate (Mao et al., 2014). A procedure for functionalizing MIL-101-Cr-NO_3 with CTAB was modified from the literature (Li et al., 2017a). All prepared MIL-101 based solids were characterized for phase identification using powder X-ray diffraction and spectroscopic analysis, and for thermal stability by thermogravimetric analysis.

MIL-101-Cr-NO_3. Chromium(III) nitrate nonahydrate (0.800 g, 2.00 mmol) and terephthalic acid (0.328 g, 1.97 mmol) were placed in a Teflon-lined autoclave followed by the addition of 4.60 mL deionized water and 0.400 mL of HNO_3 (5.00 M, 2.00 mmol). The autoclave was then sealed and placed in an oven at 210 °C for 8 h. Upon cooling, the resulting green solid was centrifuged and washed three times with dimethylformamide (DMF), water, and ethanol for 12 h at 80 °C, respectively. Detailed material characterization is described below.

MIL-101-Cr-F. Chromium(III) nitrate nonahydrate (0.400 g, 1.00 mmol) was dissolved in 4.80 mL of deionized water, and then placed in a Teflon-lined autoclave. Terephthalic acid (0.164 g, 0.987 mmol) was then added followed by the addition of 0.200 mL of HF (5.00 M, 1.00 mmol). The autoclave was then sealed and placed in an oven at 220 °C for 8 h. Upon cooling, the resulting green solid was centrifuged to collect the precipitate and solvent exchanged with DMF (3 × 10.0 mL) with centrifugation between each exchange. The product was then washed three times with DMF, water, and ethanol for 12 h at 80 °C, respectively (Skobelev et al., 2013).

MIL-101-Cr-Cl. An aqueous aluminum(III) chloride hexahydrate solution (15.0 mL, 30.0 mM) was added to a 20 mL vial containing 30.0 mg of MIL-101-Cr-F. The vial was then placed in a preheated oven at 90 °C for 18 h. Upon cooling, the resulting green solid was filtered and washed with 50.0 mL of water three times and 50.0 mL of ethanol three times.

MIL-101-Cr-I. An aqueous aluminum(III) iodide solution (15.0 mL, 30.0 mM) was added to a 20 mL vial containing 30.0 mg of MIL-101-Cr-F. The vial was then placed in a preheated oven at 90 °C for 18 h. Upon cooling, the resulting green solid was filtered and washed with 50.0 mL of water three times and 50.0 mL of ethanol three times.

MIL-101-Cr-CF_3SO_3. An aqueous aluminum(III) trifluoromethanesulfonate ($Al(CF_3SO_3)_3$) solution (15.0 mL, 30.0 mM) was added to a 20 mL vial containing 30.0 mg of MIL-101-Cr-F. The vial was then placed in a preheated oven at 90 °C for 18 h. Upon cooling, the resulting green solid was filtered and washed with 50.0 mL of water three times and 50.0 mL of ethanol three times.

MIL-101-Cr-NO_3-CTAB. Under a nitrogen atmosphere, MIL-101-Cr-NO_3 (0.200 g), cetyltrimethylammonium bromide (0.300 g), and chloroform (10.0 mL) were added to a 75 mL

heavy-wall high-pressure flask. The flask was sealed and heated at 110 °C while stirring for 3 d. The resulting green solid was centrifuged and washed three times with chloroform (20.0 mL) and then dried under vacuum for 3 h.

2.2. Material characterization

PXRD patterns were recorded on a Rigaku Miniflex II diffractometer using Cu Kα radiation (λ = 1.5406 Å) with accelerating voltage and current of 30 kV and 15 mA, respectively. The PXRD data were collected at 2θ from 2° to 30°, with a 0.01° step size and a rate of 1°/min. EDS data was collected on a TESCAN Vega-3 SBU scanning electron microscope equipped with a backscattered electron detector and EDS capability. TGA was performed on an SDT Q600 thermogravimetric analyzer using an alumina boat as a sample holder at a heating rate of 5 °C/min. Fourier-transform infrared spectra were obtained on a PerkinElmer Spectrum 100 using an attenuated total reflection accessory.

2.3. Batch adsorption experiments

Sodium perrhenate ($NaReO_4$) was purchased from Sigma-Aldrich (St. Louis, MO, USA). A known amount of $NaReO_4$ was dissolved in artificial groundwater (AGW) to prepare a 5×10^{-3} M perrhenate stock solution, which was used for sorption experiments. AGW is a simulant of typical uncontaminated groundwater from the Department of Energy's Savannah River Site (SRS), located near Aiken, South Carolina, USA (Strom and Kaback, 1992). Batch sorption experiments for obtaining Re adsorption isotherms were conducted in the AGW under ambient atmosphere and temperature (22 °C). For each set of experiments, a sorbent-free control was included at the initial Re concentration for q_e calculation (described below in Eq. 1) and to provide an indication of Re sorption to the reaction tube during the experiment. Approximately 0.05 g of the solid and a known

156 volume of AGW were added to 15 mL polypropylene centrifuge tubes. Then, the AGW solution
157 was spiked with an appropriate amount of 5×10^{-3} M $NaReO_4$ stock AGW solution so that the 5
158 mL working solution had a Re concentration ranging from 5×10^{-5} to 5×10^{-3} M. Given the high
159 fission yield for Tc-99 and its long half-life (211,000 yrs), the Re concentrations used are relevant
160 to Tc-99 remediation scenarios. For example, the Tc-99 concentration in low level tank waste at
161 the DOE Savannah River Site (SRS) is ~2 mg/L or 2×10^{-5} M, while the highest Tc concentration
162 measured in any of the SRS high-level waste tanks was ~84 mg/L or 8.5×10^{-4} M (Stallings et al.,
163 2004).The suspensions were equilibrated on a reciprocating shaker for 6 d to remain consistent
164 with past batch experiments. For one set of batch samples, pH values were not adjusted and
165 measured to be ~4.0 after the 6 d equilibration, but for the other set of batch samples, the pH was
166 adjusted to ~9.0 daily. Each suspension was passed through 0.2 μm pore-size nylon membrane
167 syringe filters. The filtrate was acidified for preservation (2% HNO_3) and analyzed for Re by
168 inductively coupled plasma mass spectrometry (ICP-MS; NexION 300X, Perkin Elmer, Inc.) in
169 accordance with the quality assurance and quality control protocols of EPA method 6020A
170 (USEPA, 2007).

171 Similarly, batch experiments were conducted to evaluate ReO_4^- adsorption on MIL-101-Cr-
172 NO_3-CTAB in AGW in relation to reaction time, pH values, and co-existing anions, as well as
173 ReO_4^- desorption/resorption cycles. Unless specified, typical experimental conditions were:
174 $[ReO_4^-] = 5 \times 10^{-5}$ M, solid/liquid = 10 g/L, reaction time = 1 d, pH = ~4.0 (without pH
175 adjustment), and two replicates. However, it is noted that de-ionized water was used for the
176 evaluation of co-existing anions on Re adsorption. The sorption/resorption experiments were also
177 conducted using pH ~4.0 AGW with an initial ReO_4^- concentration of 5×10^{-5} M and solid/liquid

ratio of 10 g/L, while the Re desorption experiment was conducted using 1 M potassium iodide (KI) solution. KI was purchased from Fisher Scientific (Hampton, NH, USA).

2.4. Synchrotron XANES and EXAFS measurements

After the batch adsorption experiments, the solid samples were air dried and collected for spectroscopic characterization. 50.0 mg of each of the air-dried powder samples was pressed into a 6.3-mm diameter disk pellet and sealed by Kapton tape. Rhenium L_3-edge XANES and EXAFS spectra were collected using the Canadian Light Source (CLS) Biological X-ray Absorption Spectroscopy (BioXAS, 07ID-2) beamline (Saskatoon, SK, Canada). The BioXAS beamline is optimized for high sensitivity and high-resolution hard X-Ray absorption spectroscopy experiments. Double crystal Si (220) monochromator was used to scan the photon energy in the vicinity of Re L_3 absorption edge at 10535 eV. Rh-coated toroidal mirrors performed the rejection of 2^{nd} and higher harmonics and moderate beam focusing down to 0.6×2 mm^2 in the sample position with total flux in the order of 10^{12} photons/s. The experiment was carried out in the energy dispersive fluorescent mode, where the characteristic X-Ray fluorescence from Re was collected by a Canberra 32-element Ge detector and the incident by N_2-filled ionization chamber. Tungsten L_3 edge (10207 eV) absorption on the tungsten reference foil was measured with every scan for energy calibration. The CLS storage ring was operated at 140–200 mA during the measurements.

All the collected spectra were processed and analyzed using the IFEFFIT software package including Athena and Artemis (Ravel and Newville, 2005). Data from multiple scans were processed using Athena by aligning and merging the spectra followed by background subtraction using the AUTOBK algorithm. Rhenium L_3-edge EXAFS data analysis was conducted on the merged and normalized spectra using Artemis. Theoretical models were constructed with the program FEFF7 (Ravel and Newville, 2005). Sodium perrhenate was used as a reference structural

model (Atzesdorfer and Range, 1995). Fits to the Re EXAFS data were made in R space (R from 1 to 3.2 Å) and obtained by taking the Fourier transform (FT) of χ(k) (k from 2 to 14) with a k weighting of 2.

3. Results

3.1. Characterization and ReO_4^- Removal of MIL-101-Cr with Different Anions

PXRD patterns of MIL-101-Cr with various anions (i.e., NO_3^-, F^-, Cl^-, I^-, and $CF_3SO_3^-$) are shown in Fig. 2A. The PXRD patterns are in agreement with the simulated pattern of MIL-101-Cr (Zhao et al., 2015), due to the isostructural nature of the prepared frameworks. The EDS spectra of F-, Cl-, I-, and CF_3SO_3-exchanged MIL-101-Cr MOFs are shown in Fig. 2B which contain the characteristic peaks for F, Cl, I, and S, respectively, reaffirming successful preparation of the anion-exchanged MIL-101-Cr materials. The SEM images of the MIL-101-Cr with different anions are also shown in Fig. S1 (Supporting Information), which indicated the locations where the EDS spectra were collected. All these MIL-101-Cr samples were fine powder. The TGA profiles of the MIL-101-Cr with different anions possess similar features for all materials as shown in Fig. 2C and are in agreement with the literature data (Zhao et al., 2015).

Batch ReO_4^- adsorption experiments were conducted from AGW at equilibrium pH values to compare the sequestration performance among these MIL-101-Cr derivatives with different exchangeable anions. The mass of Re sorbed (q_e, mg/g) was calculated using equation 1:

$$q_e = \frac{(C_0 - C_e) \times V}{M} \quad (1)$$

where C_0 (mg/L) is the initial concentration in the control samples, C_e (mg/L) is the final concentration remaining in the solution, V is the volume of the solution (mL), and M is the mass

of the sorbent (g). Fig. 2D shows that with MIL-101-Cr-NO_3 as a baseline, MIL-101-Cr-F was slightly less effective for ReO_4^- removal; while Cl-, I-, and CF_3SO_3-exchanged MIL-101-Cr materials had improved capacity for ReO_4^- sequestration. The ranking of anion-exchanged MIL-101-Cr for ReO_4^- removal was $F^- < NO_3^- < Cl^- \approx I^- \approx CF_3SO_3^-$, which, within batch experimental uncertainty, was essentially in agreement with the so-called Hofmeister order for predicting anion partitioning or exchange in liquid/liquid systems (Custelcean and Moyer, 2007). These results can be explained in terms of ionic radius and standard Gibbs energies of hydration ($\Delta G_h°$) (Custelcean and Moyer, 2007; Darab and Smith, 1996). I^- and $CF_3SO_3^-$ have a similar ionic radius and $\Delta G_h°$ to those of ReO_4^-/TcO_4^-, which is favorable for ReO_4^- exchange in the corresponding MIL-101-Cr materials and improves the ReO_4^- removal performance. On the other hand, the ionic radius and $\Delta G_h°$ of F^- are much smaller than those of ReO_4^-/TcO_4^-, which is not favorable for ReO_4^- exchange into MIL-101-Cr-F. However, MIL-101-Cr-Cl was an exception, with the ionic radius and $\Delta G_h°$ of Cl^- smaller than those of NO_3^-, and much smaller than those of ReO_4^-/TcO_4^-, but the ReO_4^- removal capacity by MIL-101-Cr-Cl was meaningfully improved compared to that of conventional MIL-101-Cr-NO_3.

3.2. Characterization CTAB-functionalized MIL-101-Cr-NO_3

Conventional MIL-101-Cr-NO_3 was selected for CTAB functionalized based on a modified literature procedure and was further studied for its improved ReO_4^- removal capacity and binding chemistry. PXRD patterns, FTIR spectra, and TGA profiles of MIL-101-Cr-NO_3 with and without CTAB functionalization are shown in Fig. 3A, 3B, and 3C, respectively. After CTAB functionalization, the PXRD pattern remained unchanged, indicating that the derivative remained isostructural to MIL-101-Cr. Two characteristic FTIR stretches at 2861 cm^{-1} and 2925 cm^{-1} indicated the presence of CTAB (Li et al., 2008), and therefore, confirmed successful

functionalization of MIL-101-Cr-NO_3 (Campbell et al., 2004). The TGA profiles of MIL-101-Cr-NO_3 with and without CTAB functionalization possess similar features.

3.3. ReO_4^- removal of CTAB-functionalized MIL-101-Cr-NO_3

ReO_4^- Removal Isotherms. Adsorption isotherms of ReO_4^- onto MIL-101-Cr-NO_3 with and without CTAB functionalization were obtained and are shown in Fig. 4A at an equilibration pH ~4.0 and Fig. 4B at an equilibration pH ~9.0. The Langmuir isotherm model (equation 2) was used to describe the data for ReO_4^- adsorption on MIL-101-Cr-NO_3-CTAB, as shown in the inset of Fig. 4:

$$\frac{C_e}{q_e} = \frac{1}{q_{\max}} C_e + \frac{1}{K_L \times q_{\max}} \quad (2)$$

where q_e is the mass of ReO_4^- sorbed onto the sorbent at equilibrium, q_{max} is the saturation sorption capacity, C_e is the Re concentration in solution at equilibrium, and K_L is the Langmuir constant that is directly related to the binding site affinity. The obtained saturation capacity of MIL-101-Cr-NO_3-CTAB for ReO_4^- removal from AGW was 139 mg ReO_4^-/g sorbent (R^2 = 0.948) at the equilibrium pH value of ~4.0 and 39 mg ReO_4^-/g sorbent (R^2 = 0.942) at the equilibrium pH value of ~9.0. In addition, we attempted to fit Re isotherm data for MIL-101-Cr-NO_3 (without CTAB functionalization) at pH values of ~4.0 and ~9.0 to both the Langmuir and Freundlich models, but neither model produces satisfactory results with R^2 values of < 0.90. However, the saturation capacity of MIL-101-Cr-NO_3 for ReO_4^- removal from AGW was ~50 mg ReO_4^-/g sorbent at pH 4.0 and ~14 mg ReO_4^-/g sorbent at pH 9.0 (Fig. 4, red). Therefore, CTAB functionalization on MIL-101-Cr-NO_3 significantly improved its capacity for ReO_4^- removal at pH 4.0 and 9.0 AGW. It is noted that the ReO_4^- removal capacity obtained for CTAB functionalized MIL-101-Cr-NO_3 was not far behind that of NU-1000 (i.e., 210 mg ReO_4^-/g sorbent) (Drout et al., 2018); however,

several recently reported MOF or cationic organic polymer materials have demonstrated much higher sorption capacities up to 1000 mg ReO_4^-/g sorbent (Da et al., 2019; He et al., 2019; Li et al., 2017b; Liu and Han, 2020; Mei et al., 2019; Sheng et al., 2017; Sun et al., 2019; Xu et al., 2019; Zhu et al., 2017a; Zhu et al., 2017b).

Effect of Contact Time. Batch experiments to obtain Re isotherms (Fig. 4) of the MIL-101-Cr-NO_3 samples with and without CTAB functionalization were initially conducted for 6 d, based on our previous experiments. The effect of contact time of ReO_4^- with these two MOF samples was further investigated to evaluate the anion exchange rate and equilibrium time. As shown in Fig. 5A, under specified experimental conditions, ~90% of ReO_4^- in AGW was removed by MIL-101-Cr-NO_3 within 30 min, while nearly 100% of ReO_4^- in AGW was removed by CTAB functionalized MIL-101-Cr-NO_3 within 10 min. Although the kinetic rate constant was not attempted to quantify, these results indicate that CTAB functionalized MIL-101-Cr-NO_3 improves sorption kinetics and provides higher capacity for ReO_4^- removal compared to MIL-101-Cr-NO_3.

Effect of Solution pH. As shown in Fig. 5B, the ReO_4^- removal percentage diminished to nearly zero for MIL-101-Cr-NO_3 and to ~15% for MIL-101-Cr-NO_3-CTAB at pH ~10.0, which is in agreement with previous results indicating that the saturation capacity for ReO_4^- removal from pH 4.0 AGW was much higher than from pH 9.0 AGW (Fig. 4). These results may indicate that these MIL-101-Cr materials have limited applications to ReO_4^-/TcO_4^- sequestration from alkaline media such as legacy liquid nuclear waste. Furthermore, these two samples were evaluated to determine if they are effective at ReO_4^-/TcO_4^- removal from acidic aqueous media since used fuel rods are usually dissolved in highly concentrated nitric acid solutions. As shown in Fig. 5B, for both MIL-101-Cr-NO_3 samples with and without CTAB functionalization, the ReO_4^- removal capacity diminished with a decreasing pH and its removal rate was reduced to ~13% in a 3 M nitric

acid solution. These results indicate that the MIL-101-Cr-NO_3 samples become less effective for ReO_4^-/TcO_4^- removal in strongly acidic aqueous media; however, it could prove effective for ReO_4^-/TcO_4^- removal from weekly acidic to neutral aqueous media like contaminated groundwater. Although the samples recovered from the 3 M nitric acid solution were not evaluated for the hydrolytic stability, the MIL-101-Cr MOF should be stable in this acidic solution, as it has been proven to be stable in pH = 0 HCl solution for two months (Leus et al., 2016).

Effect of Competing Anions. There is generally an excess of competing anions, such as NO_3^-, CO_3^{2-}, SO_4^{2-}, and Cl^-, in contaminated environmental systems, which usually have detrimental effects on the selective sequestration of ReO_4^-/TcO_4^-. Thus, ReO_4^- removal by the two MOF samples was investigated in the presence of one of these competing anions in deionized water. Fig. 5C shows ReO_4^- removal quantity and percentage in the presence of 5 mM NO_3^-, CO_3^{2-}, SO_4^{2-} or Cl^- in comparison with de-ionized water. 5 mM of each competing anion was 100 times the concentration of ReO_4^- (i.e., 5×10^{-5} M) in the tested systems. For MIL-101-Cr-NO_3, the presence of 5 mM NO_3^-, CO_3^{2-}, or Cl^- reduced ReO_4^- removal capacity by 32%, 34%, and 23%, respectively, while the presence of 5 mM SO_4^{2-} reduced ReO_4^- removal capacity by 89%. These results indicated that MIL-101-Cr-NO_3 had moderate affinity and selectivity for ReO_4^- over NO_3^-, CO_3^{2-}, or Cl^-, but SO_4^{2-} significantly reduced the affinity and selectivity of MIL-101-Cr-NO_3 for ReO_4^- removal. On the other hand, for MIL-101-Cr-NO_3-CTAB, the presence of 5 mM NO_3^-, CO_3^{2-}, and Cl^- reduced ReO_4^- removal capacity by 7%, 5%, and 2%, respectively, while the presence of 5 mM SO_4^{2-} reduced ReO_4^- removal capacity by only 18%. These results indicate that with CTAB functionalization, MIL-101-Cr-NO_3 substantially improves sorption affinity and selectivity for ReO_4^- over all tested competing anions.

ReO_4^- Desorption and Resorption Studies. ReO_4^- desorption and resorption behavior of MIL-101-Cr-NO_3 with and without CTAB functionalization was investigated by using 1 M KI solution as an extracting agent. Fig. 5D shows ReO_4^- removal percentages of MIL-101-Cr-NO_3 and MIL-101-Cr-NO_3-CTAB during sorption/desorption cycles. Within batch experimental uncertainty, the ReO_4^- sorption/desorption of the two MOF materials were similar. Initially 92–97% of ReO_4^- was removed by the sorbent materials, then 60–62% of the anion was eluted during the first desorption step; and then ~98% of ReO_4^- was sorbed by these two MOFs during the subsequent two resorption steps. These results indicate that ReO_4^- was not completely eluted by 1 M KI solution, and after the KI desorption step, the materials remained effective for ReO_4^- removal until reaching its saturation capacity.

3.3. Characterization of CTAB-functionalized MIL-101-Cr-NO_3 after ReO_4^- reaction

PXRD, FTIR and EDS. After batch experiments, solid samples were retrieved and air-dried for further characterization to determine hydrolytic stability of the sorbents, Re chemical speciation and binding mechanisms. Fig. 6 shows PXRD patterns (A), and FTIR spectra (B) of MIL-101-Cr-NO_3-CTAB that was exposed to 5×10^{-4} M ReO_4^- in pH 4.1 and 8.5 AGW, in comparison with original MIL-101-Cr-NO_3-CTAB without ReO_4^- exposure. The PXRD patterns indicated that MIL-101-Cr-NO_3-CTAB preserved its integrity and was stable in pH 4.1 AGW; but exhibited some sign of instability in pH 8.5 AGW. However, the SEM images of MIL-101-Cr-CTAB after ReO_4^- exposure in pH 4.1 and 8.5 AGW are shown in Fig. S2 (Supporting Information), which indicated that the morphology of this sample after ReO_4^- reaction at pH 4.1 and 8.5 was little changed, but slightly different from the morphology of MIL-101-Cr-NO_3-CTAB without reaction with ReO_4^- (Fig. S1F, Supporting Information).

The resonance at ~910 cm^{-1} in the FTIR spectra of MIL-101-Cr-NO_3-CTAB exposed to ReO_4^- is a characteristic peak for ReO_4^- indicating that ReO_4^- was removed from both the pH 4.1 and 8.5 solutions and captured by the MIL-101-Cr-NO_3-CTAB samples (He et al., 2019). However, it is noted that in the sample retrieved from pH 8.5 batch experiment, there was an additional peak at ~1550 cm^{-1} and the peaks at 2861 and 2925 cm^{-1} for CTAB were stronger in intensity (Li et al., 2008), compared to the sample retrieved from the pH 4.1. The EDS spectra of these samples are shown in Fig. 6C. For MIL-101-Cr-NO_3-CTAB without ReO_4^- exposure, the peak at ~2.63 keV was Cl, due to chloroform residue, and the peak at ~1.49 keV was Br, indicating that Br^- was partially exchanged into MIL-101-Cr-NO_3 when CTAB was functionalized onto its surfaces. For MIL-101-Cr-NO_3-CTAB samples exposed to ReO_4^-, the peak at ~1.83 keV was Re, further confirming Re removal by the MOF. It is noted that the Re peak in the pH 8.5 sample is stronger than that in the pH 4.1 sample, in agreement with FTIR data. While both FTIR and EDS spectra indicated that Re loading onto the sample at pH 8.5 was higher than that in the sample at pH 4.1, this contrast the batch experimental data which indicated that the quantity of Re removed was 34 mg ReO_4^-/g sorbent on the pH 8.5 sample, and 46 mg ReO_4^-/g sorbent on the pH 4.1 sample.

Re L_3-edge XANES and EXAFS. The Re L_3-edge XANES spectra of MIL-101-Cr-NO_3 and MIL-101-Cr-NO_3-CTAB after exposure to 5×10^{-4} M ReO_4^- in pH 4.1 and 8.5 AGW are shown in Fig. 7A, in comparison with the spectrum of a standard, sodium perrhenate ($NaReO_4$). The L_3-edge absorption peaks of this MOF sample exposed to ReO_4^- were at 10535.1 eV, with another peak at about 10546.4 eV. Linear combination fitting indicated that all the Re associated with the two samples was ReO_4^-. Thus, graphical comparison and linear combination fitting clearly indicated that the sequestered Re species by MIL-101-Cr-NO_3-CTAB in AGW at an equilibrium pH of 4.1-8.5 was ReO_4^-, in agreement with FTIR.

Re L_3-edge EXAFS spectra in k-space, Fourier transform plots in R magnitude and real R of these two samples are shown in Fig. 7B, 7C, and 7D, respectively, together with the corresponding spectrum of $NaReO_4$. The experimental data are shown as dotted lines, and EXAFS fits are shown as colored lines. The fitted EXAFS parameters of these samples are summarized in Table 1. The Re L_3-edge EXAFS data of the MIL-101-Cr-NO_3-CTAB samples exposed to ReO_4^- were fitted with tetrahedral Re-O paths at a Re-O distance of 1.730 ± 0.004 Å with a coordination number of 3.8 ± 0.3. Including the second Re-O path barely improved their fitting statistics. The EXAFS data fitting of these samples was acceptable as measured by the R factor of 0.01-0.02 (Table 1). Thus, the Re L_3-edge EXAFS spectra of MIL-101-Cr-NO_3-CTAB exposed to ReO_4^- in both pH 4.1 and 8.5 AGW confirmed that the Re species associated with the sorbents was ReO_4^-. In addition, the Re L_3-edge XANES and EXAFS spectra of MIL-101-Cr with different exchangeable anions (i.e., NO_3^-, F^-, Cl^-, I^-, and $CF_3SO_3^-$) exposed to 5×10^{-4} M ReO_4^- in pH 3.5−3.8 AGW are shown in Fig. S3 (Supporting Information). The Re L_3-edge XANES and EXAFS spectra of selected MIL-101-Cr-NO_3-CTAB samples from the isotherm batch experiments are also shown in Fig. S4 (Supporting Information). All these results consistently confirmed that Re chemical speciation in the MIL-101-Cr materials studied in the present work was ReO_4^-.

4. Discussion

The determination of ReO_4^- binding chemistry in MIL-101-Cr-NO_3-CTAB is less certain. The signals beyond the first Re-O path were relatively weak in Re L_3-edge EAXFS spectra (Fig. 7). Although including the second Re-O path slightly improved their fitting statistics, it is hard to distinguish whether the Re second path was Re-O, Re-N or Re-C in this sample, because O, N and C are light scatters similarly. Likely, ReO_4^- was bound and removed by MIL-101-Cr-NO_3-CTAB through two pathways. First, ReO_4^- was ion exchanged to substitute for NO_3^-/Br^- in MIL-101-Cr-

NO_3-CTAB, as expected. Second, ReO_4^- might also be bound with the positively charged sites of CTAB, in agreement with Re desorption data (Fig. 5D). A 1 M solution of KI was able to desorb ~60% of Re sorbed on MIL-101-Cr-NO_3-CTAB, this was likely the proportion of ReO_4^- bound with the positively charged sites of CTAB, as 1 M KI has been demonstrated to desorb >90% of ReO_4^- sorbed by quaternary ammonium organoclays. The desorption mechanism is likely due to I^- ion exchange for ReO_4^- bound with quaternary ammonium ligand like CTAB (Li et al., 2019). In contrast, the portion of ReO_4^- exchanged into the MIL-101-Cr-NO_3 pores might not be effectively desorbed by 1 M KI solution. This evidence also supports that ReO_4^- is sequestered by CTAB functionalized MIL-101-Cr-NO_3 through two possible mechanisms: anion exchange with NO_3^- and a non-ion exchange binding with the ligand of the functionalized CTAB molecule.

5. Conclusions

CTAB functionalized MIL-101-Cr-NO_3 was significantly effective for ReO_4^- removal from week acid to near neutral groundwater. The ReO_4^- removal capacity was 139 mg/g, the reaction kinetics were fast, reaching full capacity within 10 minutes, and the selectivity for ReO_4^- was enhanced over co-existing competing anions (i.e., NO_3^-, CO_3^{2-}, SO_4^{2-}, and Cl^-), which was especially significant for SO_4^{2-}. ReO_4^- might be synergistically sequestered through both anion exchange with NO_3^-/Br^- and non-ion exchange binding with the positively charged ligand of the functionalized CTAB molecule. These studies suggest that functionalized MOF materials may be applied to the sequestration and remediation of $^{99}TcO_4^-$ from contaminated environmental systems with high efficiencies. It is noted that these materials were very effective at $^{99}TcO_4^-$ removal from acidic to neutral pH groundwater; however, they became less stable and effective with increased pH values in groundwater.

Acknowledgements

This work was supported by the Laboratory Directed Research and Development (LDRD) program (Grant No.: LDRD-2018-00055) within the Savannah River National Laboratory (SRNL). Work was conducted at SRNL under the U.S. Department of Energy Contract DE-AC09-96SR18500. Dr. Seaman's participation in the current research was supported through a Cooperative Agreement (DEFC09-07-SR22506) between the U. S. Department of Energy and The University of Georgia Research Foundation. This research also used the BioXAS beamline of the Canadian Light Source (CLS) that was supported by the NSERC of Canada, the NRC of Canada, the Canadian Institutes of Health Research, and the Province of Saskatchewan. N.B.S. gratefully acknowledges the support of the Center for Hierarchical Wasteform Materials (CHWM), an Energy Frontier Research Center funded by the U.S. Department of Energy, Office of Science under Award DE-SC0016574, the Dreyfus Teaching-Scholar Award supported by the Dreyfus foundation, and the Sloan Research Fellowship provided by the Alfred P. Sloan foundation.

Supporting Information

The Supporting Information related to this article can be found, on the online version, at DOI,

A figure showing scanning electron microscopy images of MIL-101-Cr with different anions and CTAB functionalized MIL-101-Cr-NO_3 (Fig. S1). A figure showing scanning electron microscopy (SEM) images of MIL-101-Cr-CTAB after ReO_4^- adsorption from pH 4.1 and 8.5 artificial groundwater (Fig. S2). A figure showing Re L_3-edge X-ray absorption spectra of MIL-101-Cr with different anions after exposure to 5×10^{-4} M ReO_4^- in artificial groundwater at pH ~4.0 (Fig. S3). A figure showing Re L_3-edge X-ray absorption spectra of MIL-101-Cr-NO_3-CTAB after exposure to ReO_4^- of varying concentrations in artificial groundwater at pH ~4.0 and ~9.0 (Fig. S4).

References

Asmussen, R. M., Pearce, C. I., Miller, B. W., Lawter, A. R., Neeway, J. J., Lukens, W. W., Bowden, M. E., Miller, M. A., Buck, E. C., Serne, R. J., and Qafoku, N. P. (2018). Getters for improved technetium containment in cementitious waste forms. *J. Hazard. Mater.* 341, 238-247.

Atzesdorfer, A., and Range, K. J. (1995). Sodium metaperrhenate, NaReO4 - High-pressure synthesis of single-crystals and structure refinement. *Zeits. Naturf. Sect. B - J. Chem. Sci.* 50, 1417-1418.

Banerjee, D., Elsaidi, S. K., Aguila, B., Li, B. Y., Kim, D., Schweiger, M. J., Kruger, A. A., Doonan, C. J., Ma, S. Q., and Thallapally, P. K. (2016a). Removal of pertechnetate-related oxyanions from solution using functionalized hierarchical porous frameworks. *Chem. Euro. J.* 22, 17581-17584.

Banerjee, D., Kim, D., Schweiger, M. J., Kruger, A. A., and Thallapally, P. K. (2016b). Removal of TcO_4^- ions from solution: Materials and future outlook. *Chem. Soc. Rev.* 45, 2724-2739.

Banerjee, D., Xu, W. Q., Nie, Z. M., Johnson, L. E. V., Coghlan, C., Sushko, M. L., Kim, D., Schweiger, M. J., Kruger, A. A., Doonan, C. J., and Thallapally, P. K. (2016c). Zirconium-based metal-organic framework for removal of perrhenate from water. *Inorg. Chem.* 55, 8241-8243.

Bosch, M., Zhang, M., and Zhou, H. C. (2014). Increasing the stability of metal–organic frameworks. *Adv. Chem.* 2014, 182327.

Campbell, R. A., Parker, S. R. W., Day, J. P. R., and Bain, C. D. (2004). External reflection FTIR spectroscopy of the cationic surfactant hexadecyltrimethylammonium bromide (CTAB) on an overflowing cylinder. *Langmuir* 20, 8740-8753.

Custelcean, R., and Moyer, B. A. (2007). Anion separation with metal-organic frameworks. *Euro. J. Inorg. Chem.*, 1321-1340.

Da, H. J., Yang, C. X., and Yan, X. P. (2019). Cationic covalent organic nanosheets for rapid and selective capture of perrhenate: An analogue of radioactive pertechnetate from aqueous solution. *Environ. Sci. Technol.* 53, 5212-5220.

Daniels, N., Franzen, C., Murphy, G. L., Kvashnina, K., Petrov, V., Torapava, N., Bukaemskiy, A., Kowalski, P., Si, H., Ji, Y., Holzer, A., and Walther, C. (2019). Application of layered double hydroxides for Tc-99 remediation. *Appl. Clay Sci.* 176, 1-10.

Darab, J. G., Amonette, A. B., Burke, D. S. D., Orr, R. D., Ponder, S. M., Schrick, B., Mallouk, T. E., Lukens, W. W., Caulder, D. L., and Shuh, D. K. (2007). Removal of pertechnetate from simulated nuclear waste streams using supported zerovalent iron. *Chem. Mater.* 19, 5703-5713.

Darab, J. G., and Smith, P. A. (1996). Chemistry of technetium and rhenium species during low-level radioactive waste vitrification. *Chem. Mater.* 8, 1004-1021.

Deng, S. Q., Mo, X. J., Zheng, S. R., Jin, X., Gao, Y., Cai, S. L., Fan, J., and Zhang, W. G. (2019). Hydrolytically stable nanotubular cationic metal-organic framework for rapid and efficient removal of toxic oxo-anions and dyes from water. *Inorg. Chem.* 58, 2899-2909.

Desai, A. V., Manna, B., Karmakar, A., Sahu, A., and Ghosh, S. K. (2016). A water-stable cationic metal-organic framework as a dual adsorbent of oxoanion pollutants. *Angew. Chem. Internat. Edit.* 55, 7811-7815.

Dickson, J. O., Harsh, J. B., Lukens, W. W., and Pierce, E. M. (2015). Perrhenate incorporation into binary mixed sodalites: The role of anion size and implications for technetium-99 sequestration. *Chem. Geol.* 395, 138-143.

Ding, M., Chen, L., Xu, Y. W., Chen, B., Ding, J., Wu, R. L., Huang, C., He, Y., Jin, Y. D., and Xia, C. Q. (2020). Efficient capture of Tc/Re(VII, IV) by a viologen-based organic polymer containing tetraaza macrocycles. *Chem. Eng. J.* 380: 122581.

Dolgopolova, E. A., Rice, A. M., and Shustova, N. B. (2018). Actinide-based MOFs: A middle ground in solution and solid-state structural motifs. *Chem. Commun.* 54, 6472-6483.

Drout, R. J., Otake, K., Howarth, A. J., Islamoglu, T., Zhu, L., Xiao, C. L., Wang, S., and Farha, O. K. (2018). Efficient capture of perrhenate and pertechnetate by a mesoporous Zr metal-organic framework and examination of anion binding motifs. *Chem. Mater.* 30, 1277-1284.

Fan, D. M., Anitori, R. P., Tebo, B. M., Tratnyek, P. G., Pacheco, J. S. L., Kukkadapu, R. K., Engelhard, M. H., Bowden, M. E., Kovarik, L., and Arey, B. W. (2013). Reductive sequestration of pertechnetate $^{99}TcO_4^-$ by nano zerovalent iron (nZVI) transformed by abiotic sulfide. *Environ. Sci. Technol.* 47, 5302-5310.

Fei, H., Bresler, M. R., and Oliver, S. R. J. (2011). A new paradigm for anion trapping in high capacity and selectivity: Crystal-to-crystal transformation of cationic materials. *J. Am. Chem. Soc.* 133, 11110-11113.

Furukawa, H., Cordova, K. E., O'Keeffe, M., and Yaghi, O. M. (2013). The Chemistry and Applications of Metal-Organic Frameworks. *Science* 341, Article 1230444.

Furukawa, H., Ko, N., Go, Y. B., Aratani, N., Choi, S. B., Choi, E., Yazaydin, A. O., Snurr, R. Q., O'Keeffe, M., Kim, J., and Yaghi, O. M. (2010). Ultrahigh porosity in metal-organic frameworks. *Science* 329, 424-428.

Gu, B. H., Brown, G. M., Bonnesen, P. V., Liang, L. Y., Moyer, B. A., Ober, R., and Alexandratos, S. D. (2000). Development of novel bifunctional anion exchange resins with improved selectivity for pertechnetate sorption from contaminated groundwater. *Environ. Sci. Technol.* 34, 1075-1080.

He, L. W., Liu, S. T., Chen, L., Dai, X., Li, J., Zhang, M. X., Ma, F. Y., Zhang, C., Yang, Z. X., Zhou, R. H., Chai, Z. F., and Wang, S. (2019). Mechanism unravelling for ultrafast and selective $^{99}TcO_4^-$ uptake by a radiation-resistant cationic covalent organic framework: a combined radiological experiment and molecular dynamics simulation study. *Chem. Sci.* 10, 4293-4305.

Howarth, A. J., Katz, M. J., Wang, T. C., Platero-Prats, A. E., Chapman, K. W., Hupp, J. T., and Farha, O. K. (2015a). High efficiency adsorption and removal of selenate and selenite from water using metal-organic frameworks. *J. Am. Chem. Soc.* 137, 7488-7494.

Howarth, A. J., Liu, Y. Y., Hupp, J. T., and Farha, O. K. (2015b). Metal-organic frameworks for applications in remediation of oxyanion/cation-contaminated water. *Crystengcomm* 17, 7245-7253.

Howarth, A. J., Liu, Y. Y., Li, P., Li, Z. Y., Wang, T. C., Joseph T. Hupp, J. T., and Farha, O. K. (2016a). Chemical, thermal and mechanical stabilities of metal–organic frameworks. *Nat. Rev. Mater.* 1, 1-15.

Howarth, A. J., Peters, A. W., Vermeulen, N. A., Wang, T. C., Hupp, J. T., and Farha, O. K. (2017). Best practices for the synthesis, activation, and characterization of metal-organic frameworks. *Chem. Mater.* 29, 26-39.

514 Howarth, A. J., Wang, T. C., Al-Juaid, S. S., Aziz, S. G., Hupp, J. T., and Farha, O. K. (2016b).
515 Efficient extraction of sulfate from water using a Zr-metal-organic framework. *Dalton*
516 *Trans.* 45, 93-97.
517 Icenhower, J. P., Qafoku, N. P., Zachara, J. M., and Martin, W. J. (2010). The biogeochemistry of
518 technetium: A review of the behavior of an artificial element in the natural environment.
519 *Am. J. Sci.* 310, 721-752.
520 Leus, K., Bogaerts, T., De Decker, J., Depauw, H., Hendrickx, K., Vrielinck, H., Van Speybroeck,
521 V., and Van Der Voort, P. (2016). Systematic study of the chemical and hydrothermal
522 stability of selected "stable" Metal Organic Frameworks. *Microporous Mesoporous Mater.*
523 226, 110-116.
524 Li, B. Y., Dong, X. L., Wang, H., Ma, D. X., Tan, K., Jensen, S., Deibert, B. J., Butler, J., Cure,
525 J., Shi, Z., Thonhauser, T., Chabal, Y. J., Han, Y., and Li, J. (2017a). Capture of organic
526 iodides from nuclear waste by metal-organic framework-based molecular traps. *Nat.*
527 *Commun.* 8: 485.
528 Li, D., Seaman, J. C., Kaplan, D. I., Heald, S. M., and Sun, C. J. (2019). Pertechnetate (TcO_4^-)
529 sequestration from groundwater by cost-effective organoclays and granular activated
530 carbon under oxic environmental conditions. *Chem. Eng. J.* 360, 1-9.
531 Li, J., Dai, X., Zhu, L., Xu, C., Zhang, D., Silver, M. A., Li, P., Chen, L. H., Li, Y. Z., Zuo, D. W.,
532 Zhang, H., Xiao, C. L., Chen, J., Diwu, J., Farha, O. K., Albrecht-Schmitt, T. E., Chai, Z.
533 F., and Wang, S. A. (2018). $^{99}TcO_4^-$ remediation by a cationic polymeric network. *Nat.*
534 *Commun.* 9: 3007.
535 Li, J. R., Sculley, J., and Zhou, H. C. (2012). Metal–organic frameworks for separations. *Chem.*
536 *Rev.* 112, 869-932.
537 Li, Y. X., Yang, Z. X., Wang, Y. L., Bai, Z. L., Zheng, T., Dai, X., Liu, S. T., Gui, D. X., Liu, W.,
538 Chen, M., Chen, L. H., Diwu, J., Zhu, L. Y., Zhou, R. H., Chai, Z. F., Albrecht-Schmitt, T.
539 E., and Wang, S. (2017). A mesoporous cationic thorium-organic framework that rapidly
540 traps anionic persistent organic pollutants. *Nat. Commun.* 8: 1354.
541 Li, Z. H., Jiang, W. T., and Hong, H. L. (2008). An FTIR investigation of
542 hexadecyltrimethylammonium intercalation into rectorite. *Spectrochim. Acta Part A* 71,
543 1525–1534.
544 Liu, J., Pearce, C. I., Qafoku, O., Arenholz, E., Heald, S. M., and Rosso, K. M. (2012). Tc(VII)
545 reduction kinetics by titanomagnetite ($Fe_{3-x}Ti_xO4$) nanoparticles. *Geochim. Cosmochim.*
546 *Acta* 92, 67-81.
547 Liu, Z. W., and Han, B. H. (2020). Evaluation of an imidazolium-based porous organic polymer
548 as radioactive waste scavenger. *Environ. Sci. Technol.* 54, 216-224.
549 Mao, C. Y., Kudla, R. A., Zuo, F., Zhao, X., Mueller, L. J., Bu, X. H., and Feng, P. Y. (2014).
550 Anion stripping as a general method to create cationic porous framework with mobile
551 anions. *J. Am. Chem. Soc.* 136, 7579-7582.
552 McBeth, J. M., Lloyd, J. R., Law, G. T. W., Livens, F. R., Burke, I. T., and Morris, K. (2011).
553 Redox interactions of technetium with iron-bearing minerals. *Mineral. Mag.* 75, 2419-
554 2430.
555 Meena, A. H., and Arai, Y. (2017). Environmental geochemistry of technetium. *Environ. Chem.*
556 *Lett.* 15, 241-263.
557 Mei, L., Li, F. Z., Lan, J. H., Wang, C. Z., Xu, C., Deng, H., Wu, Q. Y., Hu, K. Q., Wang, L.,
558 Chai, Z. F., Chen, J., Gibson, J. K., and Shi, W. Q. (2019). Anion-adaptive crystalline
559 cationic material for $^{99}TcO_4^-$ trapping. *Nat. Commun.* 10: 1532.

Mon, M., Bruno, R., Ferrando-Soria, J., Armentano, D., and Pardo, E. (2018). Metal-organic framework technologies for water remediation: towards a sustainable ecosystem. *J. Mater. Chem. A* 6, 4912-4947.

Pearce, C. I., Icenhower, J. P., Asmussen, R. M., Tratnyek, P. G., Rosso, K. M., Lukens, W. W., and Qafoku, N. P. (2018). Technetium stabilization in low-solubility sulfide phases: A review. *ACS Earth Space Chem.* 2, 532-547.

Pierce, E. M., Lilova, K., Missimer, D. M., Lukens, W. W., Wu, L. L., Fitts, J., Rawn, C., Huq, A., Leonard, D. N., Eskelsen, J. R., Woodfield, B. F., Jantzen, C. M., and Navrotsky, A. (2017). Structure and thermochemistry of perrhenate sodalite and mixed guest perrhenate/pertechnetate sodalite. *Environ. Sci. Technol.* 51, 997-1006.

Pierce, E. M., Serne, R. J., Um, W., Mattigod, S. V., Icenhower, J. P., Qafoku, N. P., Westsik, J., J.H., and Scheele, R. D. (2010). "Review of Potential Candidate Stabilization Technologies for Liquid and Solid Secondary Waste Streams, PNNL-19122," Pacific Northwest National Laboratory, Richland, Washington 99352.

Plymale, A. E., Fredrickson, J. K., Zachara, J. M., Dohnalkova, A. C., Heald, S. M., Moore, D. A., Kennedy, D. W., Marshall, M. J., Wang, C. M., Resch, C. T., and Nachimuthu, P. (2011). Competitive reduction of pertechnetate $^{99}TcO_4^-$ by dissimilatory metal reducing bacteria and biogenic Fe(II). *Environ. Sci. Technol.* 45, 951-957.

Rapti, S., Diamantis, S. A., Dafnomili, A., Pournara, A., Skliri, E., Armatas, G. S., Tsipis, A. C., Spanopoulos, I., Malliakas, C. D., Kanatzidis, M. G., Plakatouras, J. C., Noli, F., Lazarides, T., and Manos, M. J. (2018). Exceptional TcO_4^- sorption capacity and highly efficient ReO_4^- luminescence sensing by Zr^{4+} MOFs. *J. Mater. Chem. A* 6, 20813-20821.

Ravel, B., and Newville, M. (2005). Athena, Artemis, Hephaestus: data analysis for X-ray absorption spectroscopy using IFEFFIT. *J. Synchrotron Radiat.* 12, 537−541.

Samanta, P., Chandra, P., Dutta, S., Desai, A., and Ghosh, S. K. (2018). Chemically stable ionic viologen-organic network: an efficient scavenger of toxic oxo-anions from water. *Chem. Sci.* 9, 7874-7881.

Shen, J., Chai, W., Wang, K. X., and Zhang, F. (2017). Efficient removal of anionic radioactive pollutant from water using ordered urea-functionalized mesoporous polymeric nanoparticle. *ACS Appl. Mater. Interfaces* 9, 22440-22448.

Sheng, D. P., Zhu, L., Dai, X., Xu, C., Li, P., Pearce, C. I., Xiao, C. L., Chen, J., Zhou, R. H., Duan, T., Farha, O. K., Chai, Z. F., and Wang, S. (2019). Successful decontamination of $^{99}TcO_4^-$ in groundwater at legacy nuclear sites by a cationic metal-organic framework with hydrophobic pockets. *Angew. Chem. Internat. Edit.* 58, 4968-4972.

Sheng, D. P., Zhu, L., Xu, C., Xiao, C. L., Wang, Y. L., Wang, Y. X., Chen, L. H., Diwu, J., Chen, J., Chai, Z. F., Albrecht-Schmitt, T. E., and Wang, S. A. (2017). Efficient and selective uptake of TcO_4^- by a cationic metal-organic framework material with open Ag^+ Sites. *Environ. Sci. Technol.* 51, 3471-3479.

Skobelev, I. Y., Sorokin, A. B., Kovalenko, K. A., Fedin, V. P., and Kholdeeva, O. A. (2013). Solvent-free allylic oxidation of alkenes with O_2 mediated by Fe- and Cr-MIL-101. *J. Catal.* 298, 61-69.

Stallings, M. E., Barnes, M. J., Peters, T. B., Diprete, D. P., Fondeur, F. F., Hobbs, D. T., and Fink, S. D. (2004). "Characterization of Supernate Samples from High Level Waste Tanks 13H, 30H, 37H, 39H, 45F, 46F and 49H, WSRC-TR-2004-00386 Revision 2," Westinghouse Savannah River Company, Aiken, SC 29808.

Strom, R. N., and Kaback, D. S. (1992). "SRP Baseline Hydrogeologic Investigation: Aquifer Characterization. Groundwater Geochemistry of the Savannah River Site and Vicinity, WSRC-RP-92-450," Westinghouse Savannah River Company, Environmental Sciences Section, Aiken, SC.

Sun, Q., Zhu, L., Aguila, B., Thallapally, P. K., Xu, C., Chen, J., Wang, S., Rogers, D., and Ma, S. Q. (2019). Optimizing radionuclide sequestration in anion nanotraps with record pertechnetate sorption. *Nat. Commun.* 10: 1646.

Um, W., Chang, H. S., Icenhower, J. P., Lukens, W. W., Serne, R. J., Qafoku, N. P., Westsik, J. H., Buck, E. C., and Smith, S. C. (2011). Immobilization of 99-technetium (VII) by Fe(II)-goethite and limited reoxidation. *Environ. Sci. Technol.* 45, 4904-4913.

USEPA (2007). Method 6020A, Rev. 0. Inductively coupled plasma-mass spectrometry. . *In* "Test Methods for Evaluating Solid Waste, Physical/Chemical Methods (SW-846) ". Office of Solid Waste, Washington, DC.

Valenta, M. M., Parker, K. E., and Pierce, E. M. (2010). "Tc-99 Ion Exchange Resin Testing, PNNL-19681," Pacific Northwest National Laboratory, Richland, Washington 99352.

Wang, C. H., Liu, X. L., Demir, N. K., Chen, J. P., and Li, K. (2016). Applications of water stable metal-organic frameworks. *Chem. Soc. Rev.* 45, 5107-5134.

Xu, H., Cao, C. S., Hu, H. S., Wang, S. B., Liu, J. C., Cheng, P., Kaltsoyannis, N., Li, J., and Zhao, B. (2019). High uptake of ReO_4^- and CO_2 conversion by a radiation-resistant thorium-nickle $Th_{48}Ni_6$ nanocage-based metal-organic framework. *Angew. Chem. Internat. Edit.* 58, 6022-6027.

Yaghi, O. M., Li, H. L., Davis, C., Richardson, D., and Groy, T. L. (1998). Synthetic strategies, structure patterns, and emerging properties in the chemistry of modular porous solids. *Accounts Chem. Res.* 31, 474-484.

Zhao, T., Jeremias, F., Boldog, I., Nguyen, B., Henninger, S. K., and Janiak, C. (2015). High-yield, fluoride-free and large-scale synthesis of MIL-101(Cr). *Dalton Trans.* 44, 16791-16801.

Zhu, L., Sheng, D. P., Xu, C., Dai, X., Silver, M. A., Li, J., Li, P., Wang, Y. X., Wang, Y. L., Chen, L. H., Xiao, C. L., Chen, J., Zhou, R. H., Zhang, C., Farha, O. K., Chai, Z. F., Albrecht-Schmitt, T. E., and Wang, S. (2017a). Identifying the recognition site for selective trapping of $^{99}TcO_4^-$ in a hydrolytically stable and radiation resistant cationic metal-organic framework. *J. Am. Chem. Soc.* 139, 14873-14876.

Zhu, L., Xiao, C. L., Dai, X., Li, J., Gui, D. X., Sheng, D. P., Chen, L. H., Zhou, R. H., Chai, Z. F., Albrecht-Schmitt, T. E., and Wang, S. (2017b). Exceptional perrhenate/pertechnetate uptake and subsequent immobilization by a low-dimensional cationic coordination polymer: Overcoming the Hofmeister bias selectivity. *Environ. Sci. Technol. Lett.* 4, 316-322.

645 **Table 1.**

646 Re L_3-edge EXAFS fitting data for Re species sequestered on MIL-101-Cr-NO_3-CTAB.
647

Samples [a]	pH	Scattering path	Interatomic distance (Å)	Coordination number	Debye–Waller factor, σ^2 ($Å^2$)	ΔE_0 (eV)	R-factor
#3	8.5	Re-O1	1.730 ± 0.004	3.7 ± 0.2	0.0001 ± 0.0005	10.0 ± 1.0	0.0187
#1	4.1	Re-O1	1.730 ± 0.004	3.9 ± 0.2	0.0003 ± 0.0005	9.8 ± 0.9	0.0111
$NaReO_4$	EXAFS	Re-O1	1.731 ± 0.007	2.8 ± 0.3	0.0028 ± 0.0009		0.0038
		Re-O2	3.037 ± 0.074	4	0.0314 ± 0.0163		
	X-ray structure (Atzesdorfer and Range, 1995)	Re-O1	1.728	4			
		Re-O2	3.06	4			

[a] Amplitude was set to 0.8

648

649

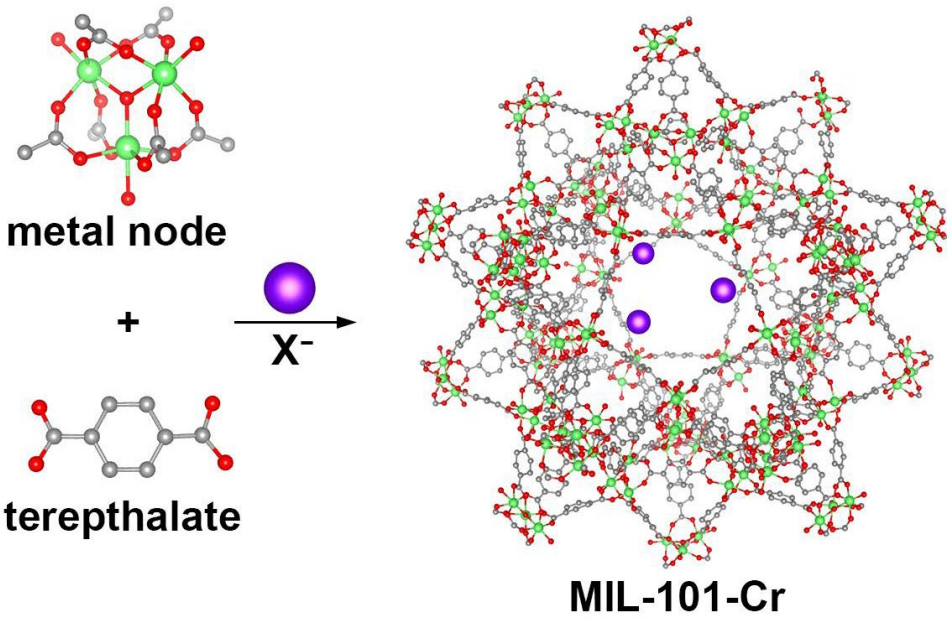

Fig. 1. The structure of MIL-101-Cr. The chromium(III) octahedral clusters are interconnected by 1,4-benzenedicarboxylates (terephthalate), resulting in a highly porous 3-dimentional structure. Atom colors: Cr = green, O = red, C = gray, blue = exchangeable anions (i.e., NO_3^-, F^-, Cl^-, I^-, and $CF_3SO_3^-$).

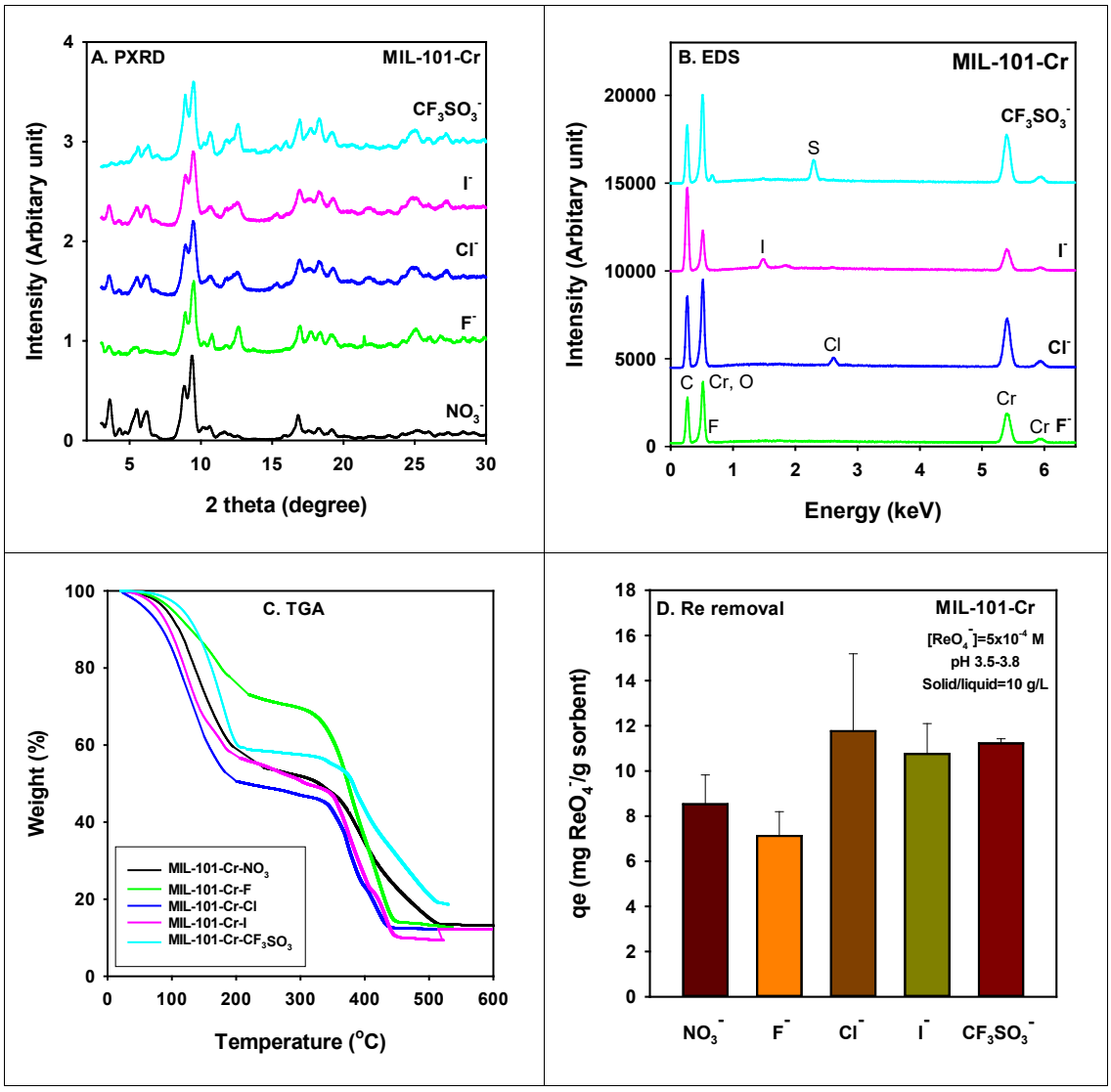

Fig. 2. PXRD (A), EDS (B), TGA (C) characterization and Re removal (D) of MIL-101-Cr with different exchangeable anions (i.e., NO_3^-, F^-, Cl^-, I^-, and $CF_3SO_3^-$).

664

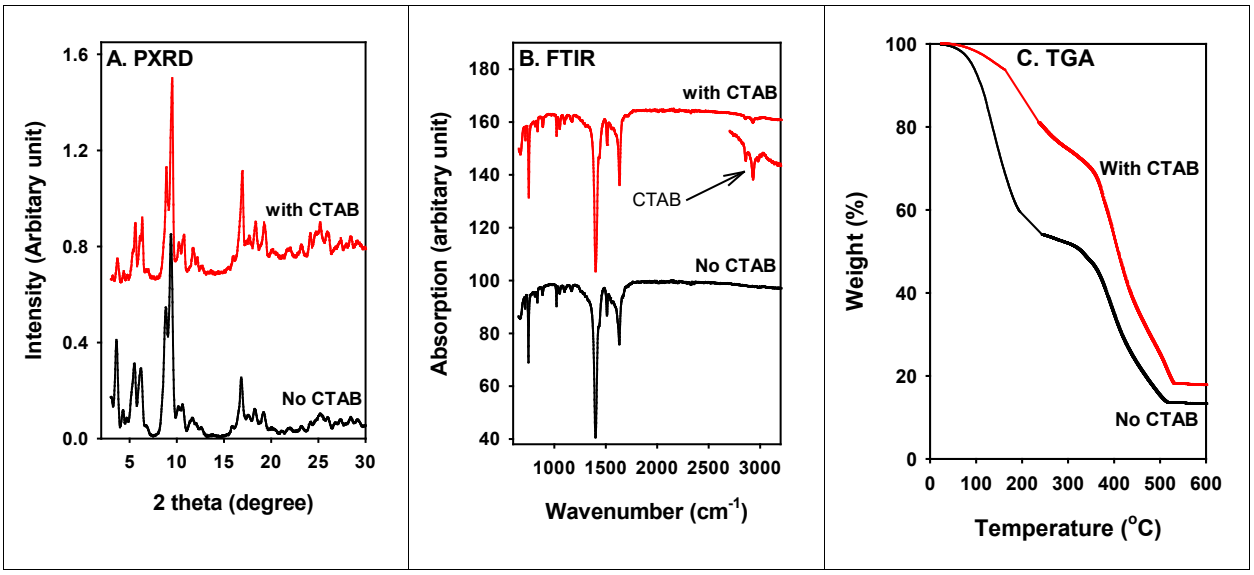

665

666 **Fig. 3.** PXRD (A), FTIR (B), and TGA (C) characterization of MIL-101-Cr-NO_3 (labeled as "No
667 CTAB") and MIL-101-Cr-NO_3-CTAB (labeled as "with CTAB").

668

669

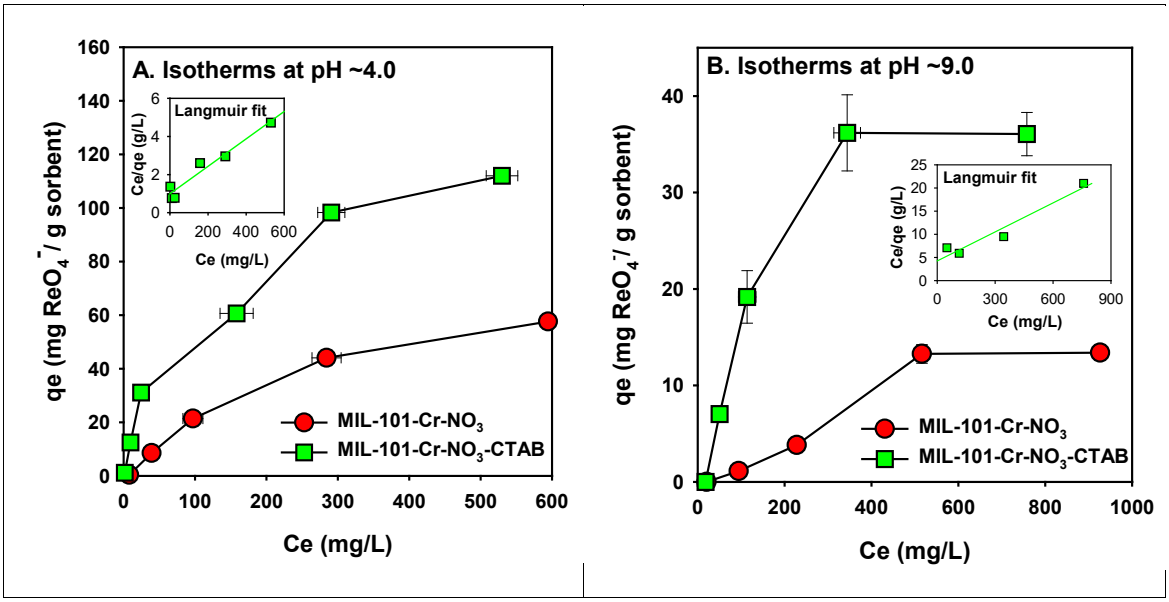

670

671 **Fig. 4.** Adsorption isotherms of ReO_4^- on MIL-101-Cr-NO_3 (red) and MIL-101-Cr-NO_3-CTAB
672 (green) in artificial groundwater at pH ~4.0 (A) and ~9.0 (B) for 6 d. All measurements represent
673 the average of two replicates. For MIL-101-Cr-NO_3-CTAB, Langmuir fits are shown in the insets,
674 but the isotherm curves for MIL-101-Cr-NO_3 were not well fit by the Langmuir model. Small error
675 bars (2 standard deviation) may be hidden by symbols.

676

677

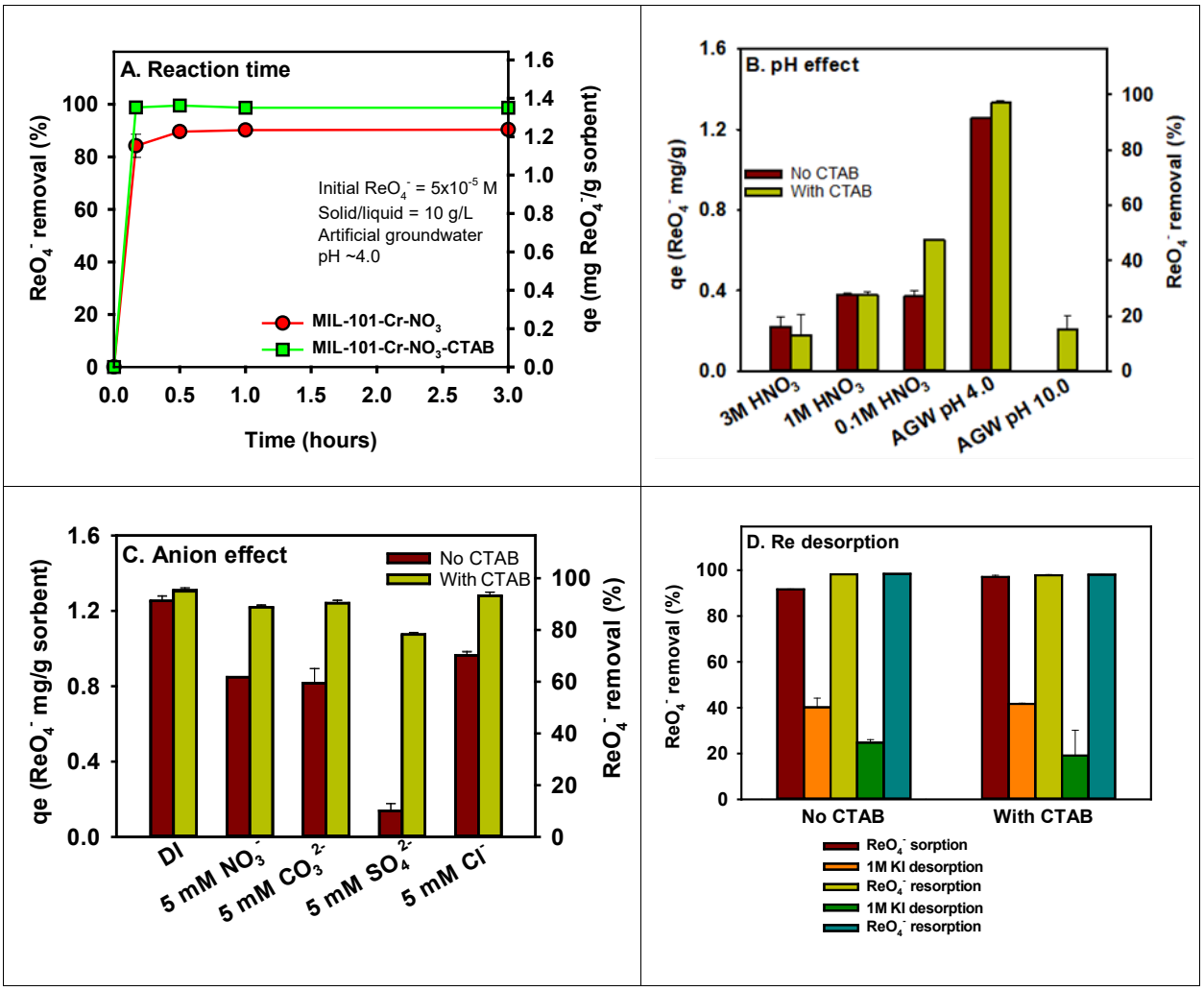

678

679 **Fig. 5.** ReO_4^- adsorption on MIL-101-Cr-NO_3-CTAB in artificial groundwater versus (A) reaction
680 time, (B) pH value (the acidic solutions were prepared using DI water), (C) co-existing anions (the
681 aqueous solutions were prepared using DI water), and (D) ReO_4^- desorption/resorption cycles. All
682 measurements represent the average of two replicates. Unless specified, the experimental
683 conditions were: $[ReO_4^-] = 5 \times 10^{-5}$ M, solid/liquid = 10 g/L, reaction time = 1 d, pH = ~4.0.

684

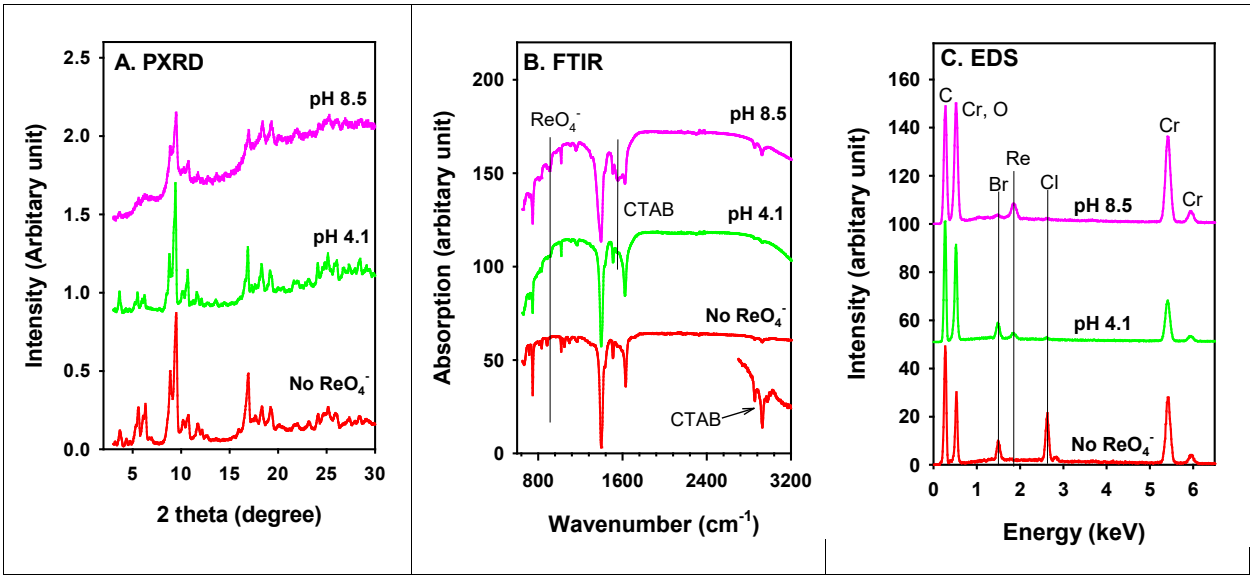

Fig. 6. PXRD (A), FTIR (B), and EDS (C) characterization of MIL-101-Cr-NO_3-CTAB before (red) and after exposure to 5×10^{-4} M ReO_4^- in artificial groundwater (AGW) at pH 4.1 (green) and 8.5 (pink).

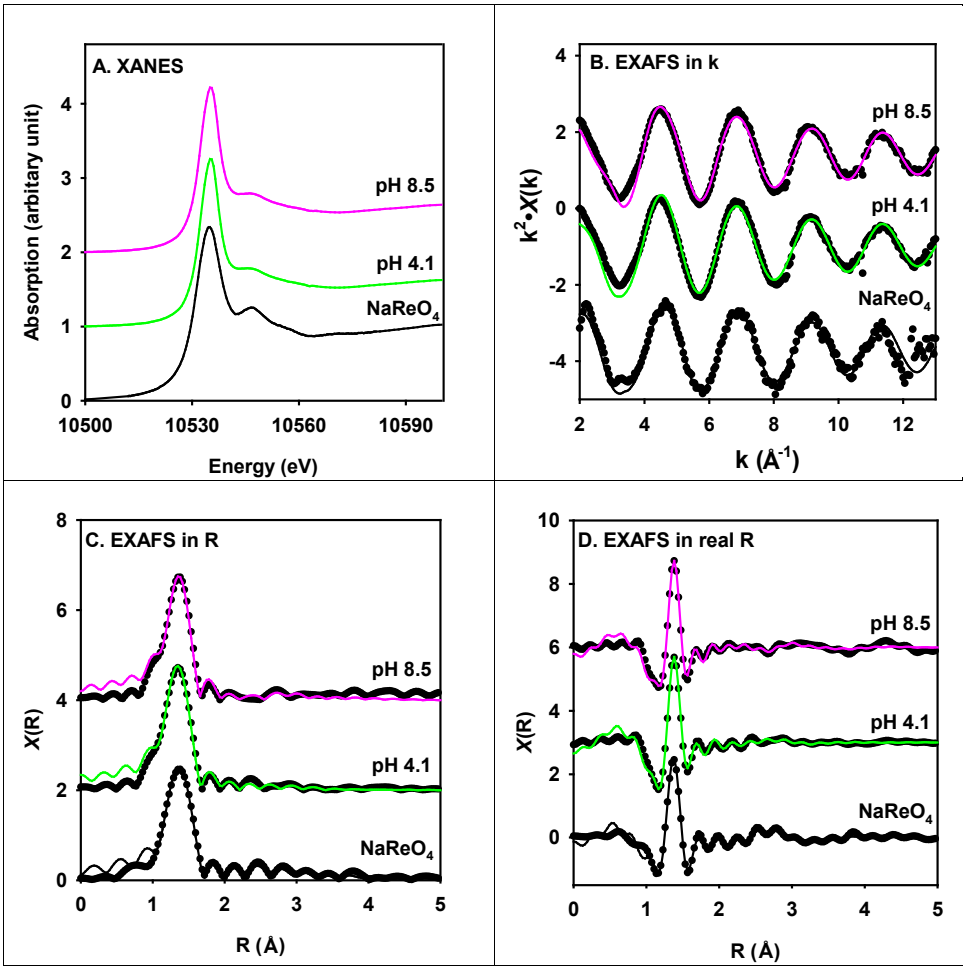

Fig. 7. Re L_3-edge X-ray absorption spectra of MIL-101-Cr-NO_3-CTAB after exposure to 5×10^{-4} M ReO_4^- in artificial groundwater at pH 4.1 (green) and 8.5 (pink), in comparison with the spectra of model compound $NaReO_4$ (black).